

HCMA: Hierarchical Cross-model Alignment for Grounded Text-to-Image Generation

Hang Wang
The Hong Kong Polytechnic
University
Hong Kong, China
cshwang@comp.polyu.edu.hk

Zhi-Qi Cheng*
University of Washington
Seattle, USA
zhiqics@uw.edu

Chenhao Lin
Xi'an Jiaotong University
Xi'an, China
linchenhao@xjtu.edu.cn

Chao Shen
Xi'an Jiaotong University
Xi'an, China
chaoshen@mail.xjtu.edu.cn

Lei Zhang
The Hong Kong Polytechnic
University
Hong Kong, China
cslzhang@comp.polyu.edu.hk

Abstract

Text-to-image synthesis has progressed to the point where models can generate visually compelling images from natural language prompts. Yet, existing methods often fail to reconcile high-level semantic fidelity with explicit spatial control, particularly in scenes involving multiple objects, nuanced relations, or complex layouts. To bridge this gap, we propose a *Hierarchical Cross-Modal Alignment* (HCMA) framework for *grounded* text-to-image generation. HCMA integrates two alignment modules into each diffusion sampling step: a *global* module that continuously aligns latent representations with textual descriptions to ensure scene-level coherence, and a *local* module that employs bounding-box layouts to anchor objects at specified locations, enabling fine-grained spatial control. Extensive experiments on the MS-COCO 2014 validation set show that HCMA surpasses state-of-the-art baselines, achieving a 0.69 improvement in Fréchet Inception Distance (FID) and a 0.0295 gain in CLIP Score. These results demonstrate HCMA's effectiveness in faithfully capturing intricate textual semantics while adhering to user-defined spatial constraints, offering a robust solution for semantically grounded image generation. Our code is available at <https://github.com/hwang-cs-ime/HCMA>

CCS Concepts

• **Computing methodologies** → **Vision and language.**

Keywords

Grounded Text-to-Image Generation, Cross-model, Semantic Alignment, Global-level and Local-level

*Corresponding author.

Permission to make digital or hard copies of all or part of this work for personal or classroom use is granted without fee provided that copies are not made or distributed for profit or commercial advantage and that copies bear this notice and the full citation on the first page. Copyrights for components of this work owned by others than the author(s) must be honored. Abstracting with credit is permitted. To copy otherwise, or republish, to post on servers or to redistribute to lists, requires prior specific permission and/or a fee. Request permissions from permissions@acm.org.
Conference'17, Washington, DC, USA

© 2018 Copyright held by the owner/author(s). Publication rights licensed to ACM.
ACM ISBN 978-1-4503-XXXX-X/2018/06
<https://doi.org/X.XX>

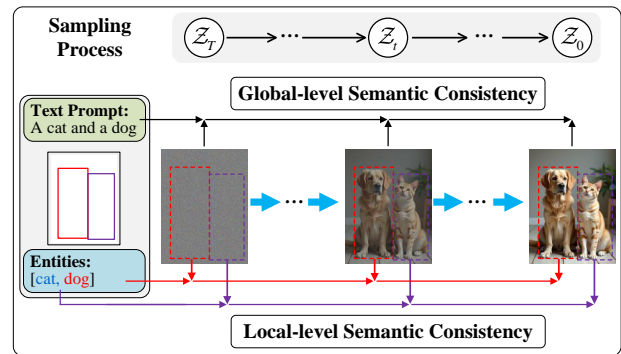


Figure 1: Overview of the HCMA Approach. In each diffusion step, HCMA's alignment ensures textual coherence globally while enforcing bounding-box layouts locally, thus providing a more robust and controllable framework for grounded text-to-image generation.

ACM Reference Format:

Hang Wang, Zhi-Qi Cheng, Chenhao Lin, Chao Shen, and Lei Zhang. 2018. HCMA: Hierarchical Cross-model Alignment for Grounded Text-to-Image Generation. In . ACM, New York, NY, USA, 10 pages. <https://doi.org/X.XX>

1 Introduction

Text-to-image synthesis [15, 23, 26, 30, 34] has witnessed rapid advancements in recent years, enabling generative models to produce visually compelling images from natural language inputs. Nevertheless, while recent approaches often yield images that appear plausible and aesthetically appealing, they still struggle to capture the full complexity of detailed or domain-specific prompts [1, 6, 33, 37]. In particular, as scenes grow more intricate—incorporating multiple objects, nuanced relationships, or fine-grained constraints—existing solutions frequently falter, underscoring the need for more powerful and controllable text-to-image frameworks.

A promising strategy for enhancing control in text-to-image generation involves specifying additional spatial constraints, especially bounding boxes that delineate where objects should appear. This approach underlies *grounded text-to-image generation*, wherein the model must simultaneously satisfy global textual semantics and explicit geometric layouts. Such grounded methods have broad utility, ranging from interactive design and storytelling [5, 12, 17, 28, 31, 35]

to augmented and virtual reality [2, 4, 13], in which precise object placement is essential for user immersion or functional coherence.

Over the past few years, various grounded text-to-image frameworks have emerged [7, 14, 21, 32, 38], often relying on specialized cross-attention mechanisms, gating modules, or other custom constraints to ensure bounding-box compliance. For example, GLI-GEN [14] integrates a gated self-attention mechanism to enhance spatial controllability, and BoxDiff [32] utilizes inner- and outer-box cross-attention constraints to adhere to user-defined object layouts. Alternatively, Attention-ReFocusing [21] harnesses GPT-4 [20] to propose object placements before refining cross-attention and self-attention layers. Despite these innovations, most existing methods do not guarantee both robust *global* text-image coherence and *local* bounding-box fidelity at every stage of the generation process. Consequently, while a system may capture the overall scene described by the text, individual regions often deviate from user-prescribed positional or categorical requirements.

To address these limitations, we present a *Hierarchical Cross-Modal Alignment* (HCMA) framework that enforces semantic consistency at both the global and local scales during grounded text-to-image generation. As detailed in Section 3 and illustrated in Figure 1, HCMA weaves two complementary alignment modules into each step of a diffusion-based sampling procedure. **(1) Global-Level (Caption-to-Image) Alignment** continuously matches the evolving latent representation with the textual prompt, thereby preserving high-level semantic coherence across the entire scene. Rather than verifying alignment only at the final step, it iteratively refines the latent space to reflect overarching themes and relationships in the text, benefiting simple captions and elaborate, multi-object prompts alike. **(2) Local-Level (Object-to-Region) Alignment** operates in parallel, leveraging bounding-box layouts to anchor each object at its designated location. At each iteration, it ensures localized latent features adhere to user-defined constraints, preventing objects from drifting away from prescribed positions or diverging from specified attributes. This layered mechanism proves especially crucial for prompts requiring strict spatial arrangements, such as non-overlapping objects or distinct, non-negotiable placements for certain categories.

By merging these two alignment processes throughout the diffusion steps, HCMA delivers both *semantic rigor* at the scene level and *precise controllability* at the object level. The global module maintains coherence with the entire textual narrative, while the local module enforces bounding-box constraints to uphold fine-grained spatial accuracy. This layered strategy effectively tackles the dual challenge of capturing a prompt’s high-level semantics and adhering to region-level instructions—requirements frequently encountered in real-world tasks like interactive storyboarding, VR world-building, or industrial design layout.

Our main contributions are as follows:

- **HCMA Framework.** We propose HCMA, a grounded text-to-image generation framework centered on *hierarchical cross-modal alignment*, ensuring both semantic fidelity and spatial controllability. By disentangling global and local alignment processes, HCMA effectively preserves textual semantics while adhering to bounding-box constraints.
- **Dual-Alignment Strategy.** We introduce a two-tiered alignment mechanism, comprising a global-level *caption-to-image* module and a local-level *object-to-region* module. Each component is optimized with distinct losses to maintain overall prompt coherence and strict, precise object placement throughout the diffusion sampling.
- **Extensive Experimental Validation.** Across the MS-COCO 2014 validation set, HCMA surpasses leading baselines, achieving a 0.69 improvement in FID and a 0.0295 gain in CLIP Score. These results confirm the framework’s effectiveness in producing images that remain coherent at the macro level while respecting bounding-box constraints at the micro level.

2 Related Work

2.1 Text-to-Image Generation

Text-to-image generation aims to synthesize images that accurately capture the semantic content of a given textual prompt [11, 18, 36, 39]. Early approaches often faced challenges in scaling to high-resolution outputs without sacrificing semantic fidelity. A major breakthrough came with the Latent Diffusion Model (LDM) [24], which projects the generation process from high-dimensional pixel space to a lower-dimensional latent space, substantially reducing computational overhead. Building on this idea, Stable Diffusion Models v1.4 and v1.5 introduced optimized sampling strategies and improved pre-trained VAEs, delivering higher-fidelity images and greater user control. Subsequent versions, such as v2, v3, and SD-XL, further refined the architecture with advanced attention mechanisms and higher-resolution capabilities, enabling more detailed and context-aware synthesis for complex prompts.

Beyond these diffusion-based models, LAFITE [40] demonstrated versatility in zero-shot and language-free scenarios by leveraging a sophisticated architecture that spans multiple semantic domains. Gafni et al. [8] incorporated human priors to improve generation quality, emphasizing salient regions and leveraging perception-level insights. Additionally, Kang et al. [10] tackled the persistent issue of object miscounting by introducing an attention map-based guidance approach, enabling high-fidelity outputs with accurate object counts dictated by the prompt. Despite these advancements, most existing methods primarily focus on global text-image coherence, often overlooking the need for precise semantic alignment at finer spatial or object-centric levels.

2.2 Grounded Text-to-Image Generation

Grounded text-to-image generation [3, 7, 21, 29, 38] extends the basic text-to-image paradigm by specifying object placements or spatial layouts alongside textual descriptions. This task requires the synthesized images to maintain overall semantic faithfulness while accurately arranging objects according to predefined bounding boxes or other geometric constraints. LoCo [38] used semantic priors embedded in padding tokens to reinforce alignment between image generation and input constraints. Layout-Guidance [7] introduced a training-free framework that modifies cross-attention layers for both forward and backward guidance, leading to fine-grained control over layout. Meanwhile, MultiDiffusion [3] formulated a numerical optimization problem based on a pre-trained diffusion model to enhance controllable image quality. Similarly,

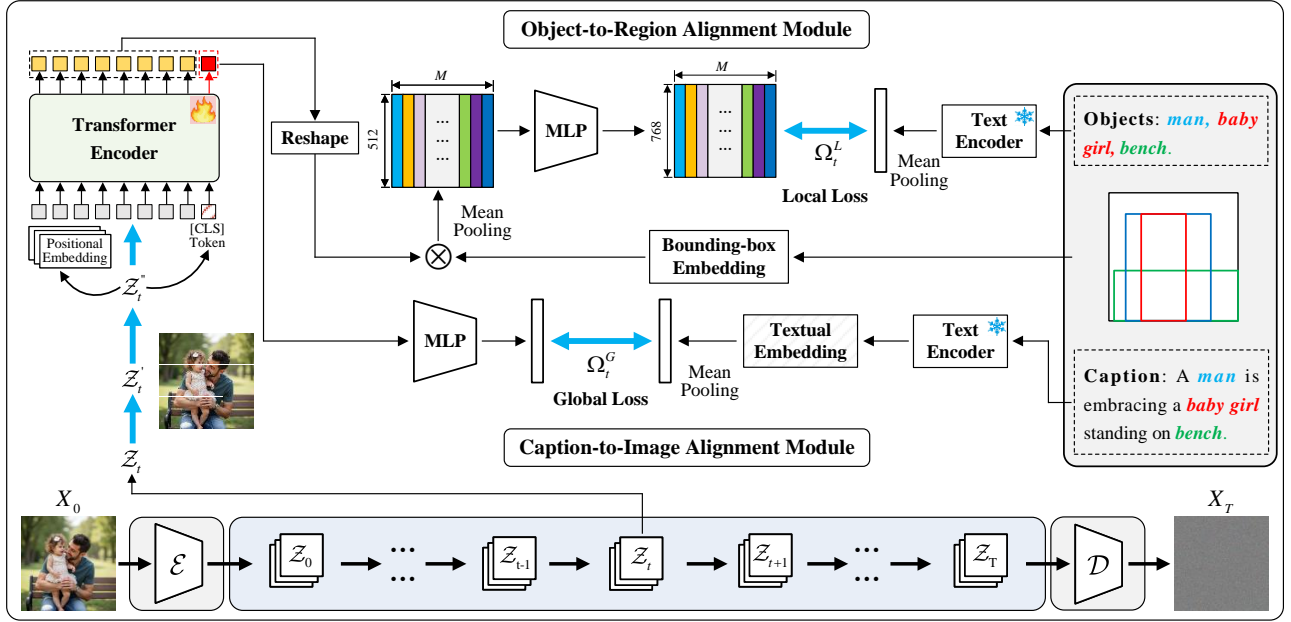


Figure 2: Training Framework of HCMA. Given a text prompt and bounding-box layouts, a *global* (caption-to-image) module fosters textual coherence while a *local* (object-to-region) module enforces bounding-box adherence. They guide the diffusion-based training so each step reflects both high-level semantics and region-specific placement.

SALT-AG [29] replaced random noise with spatially aware noise and adopted attention-guided regularization to improve layout adherence in synthesized outputs.

Although these methods achieve varying degrees of spatial controllability, most do not explicitly enforce both global text-image coherence and local object-level alignment. Our work focuses on establishing hierarchical semantic consistency at both the image and region levels, thereby achieving more robust cross-modal alignment under complex textual and spatial constraints.

3 Methodology

In this section, we introduce our proposed *Hierarchical Cross-Modal Alignment (HCMA)* framework for grounded text-to-image generation. We begin with an overview of diffusion-based image synthesis approaches and the problem setup (Section 3.1–3.2), followed by a detailed description of the HCMA model architecture and its training/inference procedures (Section 3.3).

3.1 Preliminaries

Diffusion-based methods have recently emerged as a powerful paradigm in text-to-image generation. Among these, the Latent Diffusion Model [24] (LDM) introduced the idea of operating in a learned latent space rather than raw pixel space, enabling more efficient and scalable image synthesis under various conditioning inputs (e.g., text, reference images, spatial layouts). Building on LDM, *Stable Diffusion* leverages a subset of the LAION-5B dataset [27] and employs a CLIP text encoder [22], thereby effectively bridging text and image features and substantially improving the interpretation of complex prompts and the realism of synthesized images. Formally, given a latent representation Z_t at time step t , the stable diffusion training objective aims to learn a noise estimation function ϵ_θ that

predicts the Gaussian noise ϵ added at each diffusion step:

$$\arg \min_{\theta} \|\epsilon - \epsilon_\theta(Z_t, t, f^T(c))\|^2, \quad (1)$$

where $f^T(c)$ is the CLIP embedding of c . At inference, a U-Net [25] with a spatial transformer fuses the latent representation Z_t and the text embedding c via cross-attention:

$$Q = Z_t \cdot W^Q, K = c \cdot W^K, V = c \cdot W^V, \quad (2)$$

$$\text{Attention}(Z_t, c) = \text{Softmax}\left(\frac{QK^T}{\sqrt{d}}\right) \cdot V, \quad (3)$$

where W^Q , W^K , and W^V are learnable projection matrices, and d is the channel dimension. Repeated cross-attention steps integrate textual context into the latent image features, guiding the denoising process to generate text-aligned, high-quality images.

3.2 Problem Formulation

We focus on *grounded text-to-image generation*, which aims to synthesize images that align with both textual descriptions and bounding-box constraints. Consider a noisy image X_T , a text description $c = \{c_1, c_2, \dots, c_n\}$, and a set of bounding boxes $\mathcal{B} = \{b_1, b_2, \dots, b_M\}$, where M is the number of bounding boxes. Each bounding box specifies the location of an object, whose category label y_i is encoded via CLIP to produce $f^T(y_i)$, where $y = \{y_1, \dots, y_M\}$. A pre-trained VAE transforms the noisy image X_T into a latent representation Z_T , and each box b_i is mapped to \mathbf{B} using Fourier embeddings [19].

In contrast to previous diffusion-based techniques that typically fuse text guidance and denoising in a single pass, our method partitions each diffusion step t into two complementary sub-processes,

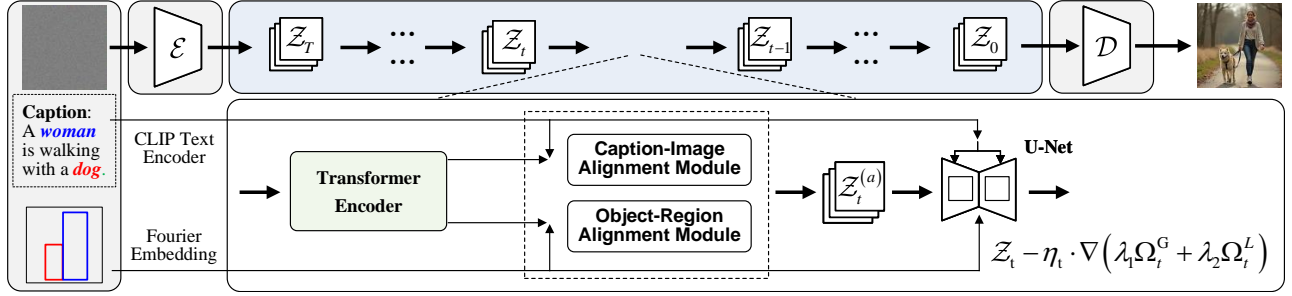


Figure 3: Sampling Process of HCMA. During inference, each diffusion step systematically alternates between refining global semantics via the caption-to-image module and strictly enforcing local bounding-box fidelity via the object-to-region module. The final image thus comprehensively unifies the textual description with explicitly defined spatial constraints.

thereby ensuring more precise alignment with both global text semantics and local object constraints. Specifically:

- (1) **Hierarchical semantic alignment**, which aligns the latent representation with both the text prompt and each bounding box’s object category. This ensures that the refined latent $Z_t^{(a)}$ respects global (image-level) semantics and local (region-level) constraints.
- (2) **Standard denoising**, in which the U-Net robustly predicts and removes the noise at step t , eventually producing Z_{t-1} from the newly aligned latent $Z_t^{(a)}$.

Mathematically, these two processes can be expressed as:

$$\begin{cases} Z_t^{(a)} = \mathcal{H}(Z_t, t, c, \mathcal{B}, y), & (4) \\ Z_{t-1} = \mathcal{G}(Z_t^{(a)}, t, f^T(c), \mathbf{B}, f^T(y), \epsilon_\theta), & (5) \end{cases}$$

where Z_t is the noisy latent at step t , $Z_t^{(a)}$ is the aligned latent after applying the alignment module \mathcal{H} , and \mathcal{G} denotes the U-Net’s denoising process. By iterating these alternating sub-processes, the model progressively refines the latent representation, ensuring that the final output respects both global textual semantics and local bounding-box specifications. This iterative refinement yields a high-quality image that remains faithful to the provided grounding conditions at each level of granularity.

3.3 HCMA Model

In this section, we introduce our *Hierarchical Cross-Modal Alignment (HCMA)* model. HCMA interleaves dedicated *alignment* and *denoising* steps during diffusion sampling to address both *global semantics* (caption-to-image) and *local layouts* (object-to-region). Through this layered alignment strategy, HCMA ensures the synthesized image preserves overarching textual consistency while affording precise spatial control over individual objects.

Overall Architecture. As illustrated in Figure 2, consider an input image $X \in \mathbb{R}^{3 \times H \times W}$, a text description $c \in \mathbb{R}^n$, and a set of bounding boxes $\mathcal{B} \in \mathbb{R}^{M \times 4}$. We extract a latent variable $Z_t \in \mathbb{R}^{4 \times \frac{H}{8} \times \frac{W}{8}}$ from a randomly chosen diffusion step t . Each bounding box b_i is transformed via a Fourier Embedding into $\mathbf{B} \in \mathbb{R}^{\frac{H}{32} \times \frac{W}{32} \times M}$. A Vision Transformer (ViT) then encodes Z_t , yielding rich multi-scale visual features, which are subsequently passed through our hierarchical alignment module consisting of:

- (1) **Caption-Image Alignment (C2IA)**: Enforces semantic coherence at a global level by aligning the latent image representation with the textual prompt.
- (2) **Object-Region Alignment (O2RA)**: Enforces spatial and categorical consistency at a local level, aligning bounding-box regions with their respective object classes.

By explicitly injecting both global and local alignment signals into the diffusion sampling procedure, HCMA achieves a balanced trade-off between holistic text-image fidelity and fine-grained control over specific visual objects.

Latent Feature Extraction. At diffusion step t , the latent Z_t is segmented and projected into $Z'_t \in \mathbb{R}^{N \times d_k}$, where $N = \frac{H}{32} \times \frac{W}{32}$ and $d_k = 64$. An MLP then transforms Z'_t into a set of visual tokens Z''_t . We prepend a learnable [CLS] token to these tokens, add positional embeddings, and feed the resulting sequence into the ViT. The ViT output naturally decomposes into two parts: a global representation $Z_t^G \in \mathbb{R}^{d_v}$, associated with the [CLS] token and capturing high-level scene semantics, and a local representation $Z_t^L \in \mathbb{R}^{N \times d_v}$, containing patch-level details for subsequent object-region alignment. *Both global and local representations serve as the basis for the hierarchical alignment mechanisms described next, ensuring the model effectively incorporates textual semantics and object-level constraints.*

3.3.1 Caption-to-Image Alignment & Global-Level Loss. Achieving overall fidelity between the synthesized image and the textual description remains a key and persistent challenge in text-to-image generation. In the absence of a robust global constraint, a model may accurately align certain local regions to segments of the text while still failing to capture the broader thematic or contextual elements of the prompt. The *Caption-to-Image Alignment (C2IA)* module addresses this shortcoming by projecting both the latent image representation and the text embedding into a shared semantic space, thereby effectively promoting holistic coherence.

Concretely, we obtain Z_t^G (the global representation) from the ViT’s [CLS] token and project it through a three-layer fully connected network, producing $f_t^G \in \mathbb{R}^{d_t}$. In parallel, the text prompt c is encoded by the CLIP text encoder, yielding $f^T(c)$. To quantify global alignment, we define:

$$\Omega_t^G = 1 - \frac{f_t^G \cdot f^T(c)}{\|f_t^G\| \|f^T(c)\|}. \quad (6)$$

Here, Ω_t^G effectively measures the inverse cosine similarity between \mathbf{f}_t^G and $f^T(c)$. By minimizing Ω_t^G , the model incrementally refines the latent image’s global features to more closely match the text embedding. Consequently, each diffusion step is guided toward producing images that reflect not only local details but also the overarching themes and context described by c .

3.3.2 Object-to-Region Alignment & Local-Level Loss. Even with robust global alignment, misplacement or misclassification of objects can occur if local constraints are overlooked. *Object-to-Region Alignment (O2RA)* addresses this by tying specific bounding-box regions to their corresponding object categories, preserving local fidelity to the textual instructions.

We reshape \mathbf{Z}_t^L into $\mathbf{Z}_t^l \in \mathbb{R}^{\frac{H}{32} \times \frac{W}{32} \times d_v}$ and fuse it with the bounding-box feature $\mathbf{B} \in \mathbb{R}^{\frac{H}{32} \times \frac{W}{32} \times M}$. This produces $\mathbf{Z}_t^{Lb} \in \mathbb{R}^{\frac{H}{32} \times \frac{W}{32} \times M \times d_v}$. After mean pooling and an MLP projection, we obtain $\mathbf{f}_t^L \in \mathbb{R}^{M \times d_l}$, where \mathbf{f}_{t,b_i}^L corresponds to the i -th bounding box. If $f^T(y_i)$ is the CLIP embedding of the label y_i , the *local-level loss* is:

$$\Omega_t^L = \frac{1}{M} \sum_{i=1}^M \left(1 - \frac{\mathbf{f}_{t,b_i}^L \cdot f^T(y_i)}{\|\mathbf{f}_{t,b_i}^L\| \|f^T(y_i)\|} \right). \quad (7)$$

Consequently, minimizing Ω_t^L drives the model to generate objects in each bounding-box region that accurately match their designated categories and spatial extents.

3.3.3 Sampling Update in Latent Space. During inference, HCMA interleaves *alignment* and *denoising* at each diffusion step t . Let \mathbf{Z}_t denote the latent representation at step t . We first apply an *alignment* update:

$$\mathbf{Z}_t^{(a)} \leftarrow \mathbf{Z}_t - \nabla \left(\lambda_1 \Omega_t^G + \lambda_2 \Omega_t^L \right) \eta_t, \quad (8)$$

where λ_1 and λ_2 balance the global and local losses, and η_t is the alignment learning rate. This step refines \mathbf{Z}_t to better satisfy both caption-to-image and object-to-region constraints. Next, we pass the updated latent $\mathbf{Z}_t^{(a)}$ to a U-Net \mathcal{G} for a *denoising* update:

$$\mathbf{Z}_{t-1} \leftarrow \mathbf{Z}_t^{(a)} - \gamma \epsilon_\theta(\mathbf{Z}_t^{(a)}, t, f^T(c), \mathbf{B}), \quad (9)$$

where γ is a step-size parameter, and ϵ_θ is the learned noise-estimation model. By iterating from $t = T$ down to $t = 0$, we perform a “dual refinement” at every step—alternating between alignment and denoising—to ultimately obtain the final latent \mathbf{Z}_0 . This refined latent is then decoded by the VAE into the synthesized image, ensuring that the output respects the textual semantics and bounding-box constraints while maintaining high visual fidelity.

3.4 Training and Inference

Algorithm 1 outlines the overall procedure. **(1)** During training, at each diffusion step t , the model computes the global and local alignment losses (Ω_t^G and Ω_t^L), updates \mathbf{Z}_t accordingly, and then applies the standard diffusion noise-prediction objective to optimize ϵ_θ . After sufficient epochs, HCMA becomes adept at integrating textual semantics and bounding-box constraints within the latent space. **(2)** At inference, \mathbf{Z}_T is randomly initialized and subjected to an *align-then-denoise* routine, iterating until it converges to a latent embedding that satisfies both the global textual prompt and

Algorithm 1 Hierarchical Cross-modal Alignment (HCMA) Training and Inference

- 1: **Input:** Text prompt c , bounding boxes $B = \{b_i\}_{i=1}^M$, object categories $y = \{y_i\}_{i=1}^M$, total denoising steps T , initial latent \mathbf{Z}_T , learning rate η_t
 - 2: **Output:** Generated image latent \mathbf{Z}_0
 - 3: **Training:**
 - 4: **for** each training step t **do**
 - 5: Encode text prompt c using CLIP text encoder: $\mathbf{f}_T(c)$
 - 6: Encode object categories y_i using CLIP: $\mathbf{f}_T(y_i)$
 - 7: Compute bounding box embedding B with Fourier encoding
 - 8: Extract visual tokens from \mathbf{Z}_t via ViT to get $\mathbf{Z}_t^G, \mathbf{Z}_t^L$
 - 9: Project \mathbf{Z}_t^G and \mathbf{Z}_t^L through MLPs to get $\mathbf{f}_t^G, \mathbf{f}_t^L$
 - 10: Compute global alignment loss: $\Omega_t^G = 1 - \cos(\mathbf{f}_t^G, \mathbf{f}_T(c))$
 - 11: Compute local alignment loss: $\Omega_t^L = \frac{1}{M} \sum_{i=1}^M \left(1 - \cos(\mathbf{f}_{t,b_i}^L, \mathbf{f}_T(y_i)) \right)$
 - 12: Compute alignment-guided latent: $\mathbf{Z}_t^{(a)} \leftarrow \mathbf{Z}_t - \eta_t \cdot \nabla(\lambda_1 \Omega_t^G + \lambda_2 \Omega_t^L)$
 - 13: Update noise prediction model ϵ_θ using noise loss $\|\epsilon - \epsilon_\theta(\mathbf{Z}_t^{(a)}, t, \mathbf{f}_T(c), B)\|^2$
 - 14: **end for**
 - 15: **Inference (Sampling):**
 - 16: Initialize latent $\mathbf{Z}_T \sim \mathcal{N}(0, I)$
 - 17: **for** $t = T$ **to** 1 **do**
 - 18: Compute Ω_t^G, Ω_t^L as in training
 - 19: Compute aligned latent: $\mathbf{Z}_t^{(a)} \leftarrow \mathbf{Z}_t - \eta_t \cdot \nabla(\lambda_1 \Omega_t^G + \lambda_2 \Omega_t^L)$
 - 20: Predict noise: $\epsilon_\theta(\mathbf{Z}_t^{(a)}, t, \mathbf{f}_T(c), B)$
 - 21: Update latent: $\mathbf{Z}_{t-1} \leftarrow \mathbf{Z}_t^{(a)} - \gamma \cdot \epsilon_\theta(\cdot)$
 - 22: **end for**
 - 23: **return** \mathbf{Z}_0
-

the specified bounding boxes. This iterative process yields a final latent state \mathbf{Z}_0 , which the VAE decodes into an image exhibiting semantic fidelity to the text and accurately placing objects as prescribed. **(3)** By integrating hierarchical cross-modal alignment into a diffusion-based sampling framework, HCMA offers a flexible and robust solution for generating images under complex textual descriptions and bounding-box layouts. It enforces caption-to-image and object-to-region constraints, mitigating issues such as object misclassification or mismatched scenes. Furthermore, by alternating alignment and denoising steps, the model incrementally incorporates textual and layout guidance, enabling reliable multi-object or multi-layout generation without sacrificing image quality.

4 Experiments

4.1 Datasets

We employ the MS-COCO 2014 dataset [16] for our experiments, comprising 82,783 images for training and 40,504 images for validation. Each image features five textual captions describing its semantic content, as well as bounding boxes and category labels for the objects present. This extensive annotation scheme offers

Methods	Image-level		Region-level	
	FID (↓)	CLIP score (↑)	FID (↓)	CLIP score (↑)
SD-v1.4 [24]	12.12	0.2917	13.66	0.2238
SD-v1.5 [24]	9.43	0.2907	13.76	0.2237
Attend-and-Excite [6]	14.87	0.2854	14.57	0.2224
BoxDiff [32]	20.26	0.2833	14.27	0.2248
Layout-Guidance [7]	21.82	0.2869	21.50	0.2262
GLIGEN (LDM) [14]	13.05	0.2891	18.53	0.2381
GLIGEN (SD-v1.4) [14]	12.07	0.2936	17.25	0.2356
HCMA(SD-v1.4)	8.74	0.3231	12.48	0.2392

Table 1: Quantitative comparison on the MS-COCO 2014 validation set, evaluated at both image-level and region-level. “SD-v1.4” and “SD-v1.5” denote backbone diffusion models v1.4 and v1.5, while “LDM” refers to the original latent diffusion model [24]. Lower FID (↓) and higher CLIP score (↑) indicate better performance, with bolded figures indicating best metrics.

a robust platform for evaluating both global-level semantic alignment and local-level object consistency in grounded text-to-image generation.

For our HCMA approach, we partition the MS-COCO 2014 training set into 80% for training and 20% for validation, maintaining consistency with standard practices in text-to-image research. Following typical protocols for grounded text-to-image generation, we then use the official MS-COCO 2014 validation set as our testing set. To enable direct comparison with prior methods and to ensure a comprehensive assessment of our framework, we sample 30,000 images from the test set to report final quantitative results.

In all experiments, we adopt the Fréchet Inception Distance (FID) [9] and CLIP score [22] to measure performance. FID quantifies the distributional similarity between real and synthesized images, while the CLIP score evaluates semantic consistency by comparing text and image embeddings within a shared feature space. Together, these metrics provide an in-depth analysis of both visual fidelity and text alignment.

4.2 Evaluation Metrics and Baselines

Fréchet Inception Distance (FID) [9]: We use FID to quantify how closely generated outputs resemble real images at a distributional level, using feature embeddings from Inception-V3. Specifically, FID computes the Fréchet distance between the mean and covariance of embeddings from the real and synthesized image sets. Lower FID values indicate greater similarity to real images, reflecting higher visual fidelity and diversity.

CLIP Score [22]: We also evaluate semantic alignment between generated images and text prompts through the CLIP model (Contrastive Language-Image Pre-training). By embedding both images and text in a shared feature space, CLIP computes the cosine similarity between generated images and their corresponding textual descriptions. Higher CLIP scores thus indicate stronger semantic consistency. For each compared method, we use a pre-trained CLIP ViT-B/32 model to ensure consistent evaluation.

Baseline Methods. We compare HCMA against seven state-of-the-art models, following their official training and validation setups on the MS-COCO 2014 dataset and evaluating on its official validation set. Table 1 presents the final results. Specifically:

- **SD-v1.4** [24], **SD-v1.5** [24], and **Attend-and-Excite** [6] are text-to-image generation methods relying solely on textual prompts.

- **BoxDiff** [32], **Layout-Guidance** [7], **GLIGEN (LDM)** [14], and **GLIGEN (SD-v1.4)** [14] are grounded text-to-image approaches that accept bounding box layouts in addition to the text prompt.

We adopt each method’s official hyperparameters to ensure fairness and reproducibility. This unified evaluation strategy allows us to rigorously assess HCMA’s performance with respect to both semantic fidelity and spatial adherence.

4.3 Implementation Details

We build HCMA upon Stable Diffusion v1.4 as our primary diffusion backbone. During training, we employ a batch size of 1024 on an HPC environment, allowing efficient parallelization. Our Vision Transformer (ViT) model consists of 8 attention heads, 6 transformer blocks, a hidden dimension of $d_v = 512$, and an input resolution of 64×64 . Training proceeds for 60 epochs using the Adam optimizer (learning rate 1×10^{-3} , weight decay 5×10^{-4}), and the hyperparameters λ_1 and λ_2 are set to 1.

Regarding the sampling process, we utilize the PLMS sampler with 50 steps. At each diffusion step, we alternate between alignment optimization and denoising, thereby ensuring that each partial update thoroughly preserves semantic integrity. This iterative procedure consistently promotes alignment across both global and local levels of the generated images. Throughout experimentation, we maintain fixed random seeds to reinforce reproducibility and systematically monitor performance at regular intervals to select stable checkpoints. Our final model thus balances alignment accuracy and computational efficiency while preserving high visual fidelity across diverse scenes and object arrangements.

4.4 Quantitative Results

Table 1 compares our HCMA framework with seven state-of-the-art baselines. Specifically, SD-v1.4, SD-v1.5, and Attend-and-Excite are text-to-image generation methods, whereas BoxDiff, Layout-Guidance, GLIGEN (LDM), and GLIGEN (SD-v1.4) address grounded text-to-image tasks. From these results, HCMA attains the highest performance in both FID and CLIP scores, indicating its effectiveness at both the image and region levels.

Image-Level Performance. Compared to SD-v1.5, HCMA improves FID by 0.69 and CLIP score by 0.0324, demonstrating enhanced semantic consistency and higher visual fidelity across generated scenes. Against the strongest grounded method, GLIGEN

C2IA	O2RA	Image-level		Region-level	
		FID (\downarrow)	CLIP score (\uparrow)	FID (\downarrow)	CLIP score (\uparrow)
		12.07	0.2936	17.25	0.2356
	✓	9.62	0.3225	11.65	0.2389
✓		9.14	0.3229	11.75	0.2386
✓	✓	8.74	0.3231	12.48	0.2392

Table 2: Ablation study on the MS-COCO 2014 validation set, showing how each alignment module (C2IA for global-level, O2RA for local-level) affects image- and region-level performance. Combining both modules yields the best FID and CLIP metrics.

(SD-v1.4), HCMA achieves gains of 3.33 in FID and 0.0295 in CLIP score. These substantial margins reflect HCMA’s capability to handle finer object interactions, complex scene composition, and detailed text instructions that other methods often struggle with. The improvements likely stem from the synergy between global semantic alignment and local bounding-box adherence, where each diffusion step benefits from both high-level coherence and precise spatial constraints.

Region-Level Performance. Focusing on local quality, HCMA surpasses SD-v1.5 by 1.28 in FID and 0.0155 in CLIP score, underscoring its prowess in preserving object integrity and aligning local semantics. Compared to GLIGEN (SD-v1.4), HCMA yields additional gains of 4.77 in FID and 0.0036 in CLIP score, highlighting the efficacy of hierarchical cross-modal alignment in enforcing strict spatial constraints without sacrificing realism. Overall, these findings confirm that unifying global (image-wide) and local (region-level) alignment enables HCMA to faithfully capture multi-object prompts and fulfill complex layout requirements in a cohesive manner.

4.5 Ablation Study

To investigate the roles of the caption-to-image alignment (C2IA) and object-to-region alignment (O2RA) modules in our proposed HCMA framework, we conduct ablation experiments by systematically disabling one or both modules. The key findings, presented in Table 2, reveal how each module contributes to both image-level and region-level performance.

4.5.1 Effectiveness of the C2IA Module. Removing C2IA focuses the entire alignment on local bounding-box adherence, leaving O2RA as the sole mechanism for enforcing semantic consistency. Consequently, the variant HCMA (w/o C2IA) aligns object categories and bounding boxes at each diffusion step, but lacks an explicit strategy to ensure global semantic coherence between the generated image and the text prompt. From Table 2, we observe that without C2IA, the FID score degrades by 0.88 and the CLIP score decreases by 0.0006 at the image level; region-level CLIP also drops by 0.0003. Despite this decline, HCMA (w/o C2IA) still achieves considerable gains over the approach missing both modules, indicating that even local alignment alone can provide meaningful improvements. However, these results underscore the importance of continuously aligning the latent representation with the textual narrative. By providing a global context, C2IA helps coordinate object arrangements, colors, and overall scene composition. Its absence causes certain scene-wide semantics to weaken, leading to lower scores.

4.5.2 Effectiveness of the O2RA Module. Analogously, omitting O2RA means only the textual prompt is aligned with the entire

image, effectively removing any explicit bounding-box alignment. Table 2 shows that this omission reduces image-level FID and CLIP by 0.4 and 0.0002, respectively, along with a region-level CLIP loss of 0.0006. Though these drops might seem modest compared to removing C2IA, they suggest that local constraints still play a pivotal role in guiding precise object placements. In fact, HCMA (w/o O2RA) remains superior to a model lacking both modules, which highlights that global semantics alone can provide partial gains. Yet, the absence of O2RA allows objects to deviate from their specified locations and attributes, limiting the method’s ability to faithfully represent complex or tightly constrained prompts.

4.5.3 Combined Analysis. Overall, these ablation results demonstrate that C2IA and O2RA fulfill complementary roles in HCMA. C2IA upholds a scene-wide semantic narrative by continuously matching the image representation to the text prompt, whereas O2RA refines individual bounding boxes to reflect their targeted content. Although each module independently boosts performance, the synergy is most evident when both are integrated: The complete HCMA model achieves the highest FID and CLIP scores at both the image and region levels. Notably, a slight trade-off emerges where global alignment can indirectly influence local generation, potentially affecting region-level fidelity, yet the net effect remains overwhelmingly positive. This interplay highlights the nuanced balance HCMA strikes between capturing the prompt’s overarching meaning and enforcing precise local constraints, ultimately yielding more coherent and spatially accurate generation.

4.6 Qualitative Analysis

Figure 4 shows a visual comparison between our HCMA framework and four baseline models, evaluated on five diverse samples that vary in complexity and object arrangements.

(1) Single Object. In the first column, focusing on a simpler single-object scenario, Attend-and-Excite introduces artifacts, whereas SD-v1.5 generates a bear with unrealistic features. Although BoxDiff is a grounded text-to-image method, it disregards the specified layout constraints. GLIGEN (SD-v1.4) places a bear in the correct location but fails to respect the exact quantity indicated by both the text prompt and bounding box. In contrast, HCMA correctly positions a bear at the predefined spot, preserving a appearance (e.g., casting a plausible shadow) and matching the required object count.

(2) Object Pair Relationships. The second and third columns depict a pair of objects that either interact or are arranged according to a prepositional relationship. Here, our HCMA approach precisely locates each distinct object in accordance with the bounding-box constraints and textual instructions, producing visually consistent

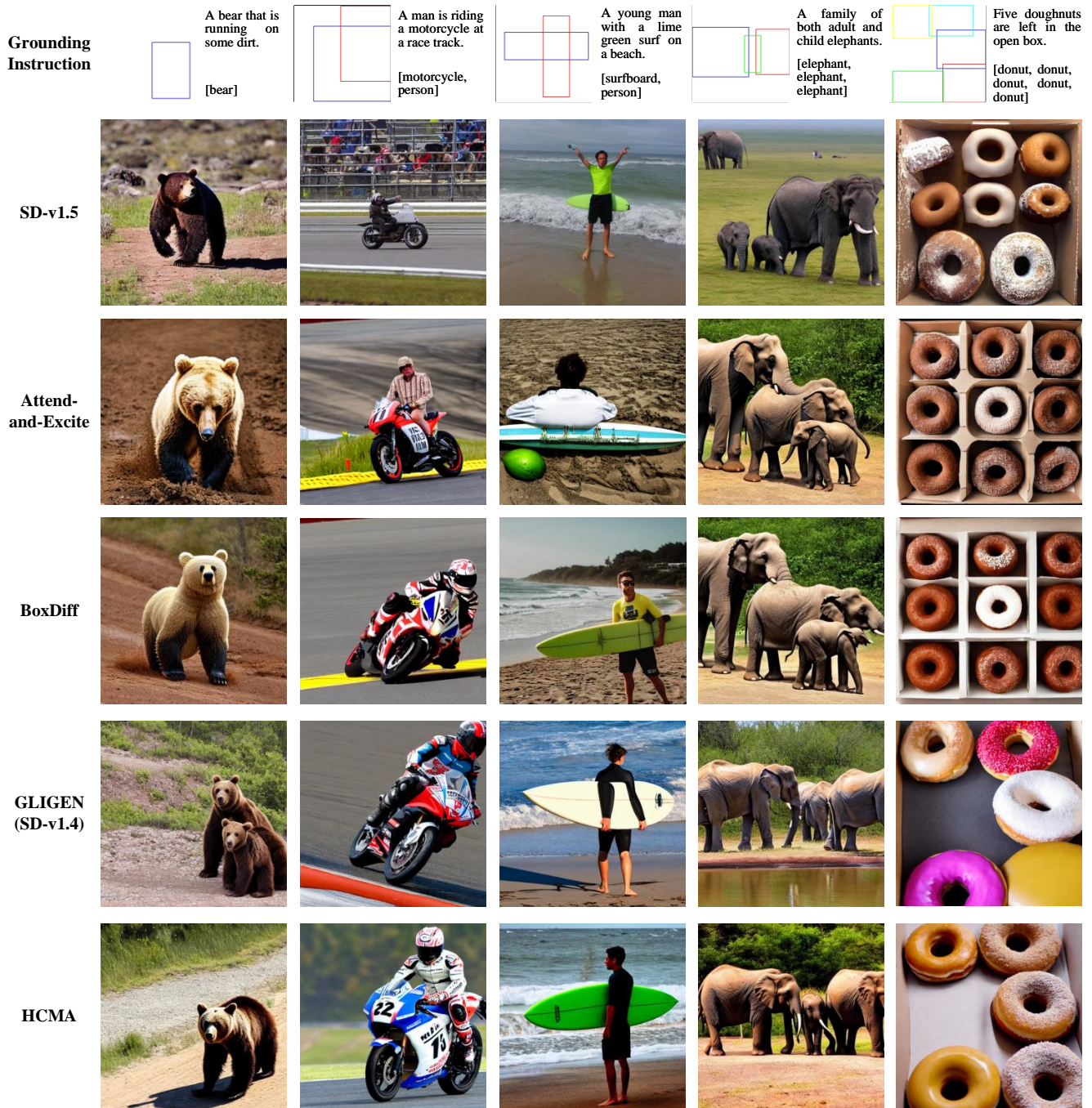


Figure 4: Visualization comparisons of different methods on the MS-COCO 2014 validation set.

scenes that exhibit minimal artifacts and maintain a lifelike quality. This outcome underscores HCMA’s capacity to handle notably more intricate spatial relationships beyond simple placements, revealing the synergy of its global and local alignment modules.

(3) Counting and Classification. In the last two columns, HCMA not only generates the correct number of objects—such as multiple elephants in the fourth column and donuts in the fifth—but also

distinguishes object categories (e.g., separating adult from child elephants). By contrast, GLIGEN (SD-v1.4) erroneously synthesizes three adult elephants in the fourth column and misclassifies baked items in the fifth column (producing four donuts plus an additional bread piece). These results emphasize HCMA’s proficiency in aligning textual instructions with both counting accuracy and fine-grained classification, while preserving high visual fidelity.

5 Conclusion

We have presented the *Hierarchical Cross-Modal Alignment* (HCMA) framework, which unifies global text-image coherence with local bounding-box adherence for grounded text-to-image generation. By alternating between caption-to-image alignment and object-to-region alignment at each diffusion step, HCMA maintains high-level semantic fidelity while enforcing precise region-specific constraints. Experiments on the MS-COCO 2014 validation set show significant gains in FID and CLIP Score over state-of-the-art baselines, indicating that this layered alignment approach effectively addresses the shortcomings of methods focusing solely on global semantics or local placement. Looking ahead, HCMA could be extended by incorporating additional modalities (e.g., depth maps, reference images) to enrich layout control, or by using adaptive weighting between global and local modules to handle varying prompt complexities and domain-specific needs. Future work may also include human-in-the-loop feedback, domain adaptation for specialized datasets, or real-time interactive adjustments, further enhancing HCMA's applicability to scenarios like virtual prototyping, creative media design, and immersive storytelling. Ultimately, HCMA offers a robust, flexible basis for tasks demanding both overarching textual fidelity and precise spatial configuration, paving the way for more advanced and controllable generative models.

References

- [1] Aishwarya Agarwal, Srikrishna Karanam, KJ Joseph, Apoorv Saxena, Koustava Goswami, and Balaji Vasani Srinivasan. 2023. A-star: Test-time attention segregation and retention for text-to-image synthesis. In *Proceedings of the IEEE/CVF International Conference on Computer Vision*. 2283–2293.
- [2] Xupeng Ai, Victor Santamaria, and Sunil K Agrawal. 2024. Characterizing the effects of adding virtual and augmented reality in robot-assisted training. *IEEE Transactions on Neural Systems and Rehabilitation Engineering* (2024).
- [3] Omer Bar-Tal, Lior Yariv, Yaron Lipman, and Tali Dekel. 2023. MultiDiffusion: fusing diffusion paths for controlled image generation. In *Proceedings of the 40th International Conference on Machine Learning* (Honolulu, Hawaii, USA) (ICML '23). JMLR.org, Article 74, 16 pages.
- [4] Tara Boroushaki, Maisy Lam, Laura Dodds, Aline Eid, and Fadel Adib. 2023. Augmenting Augmented Reality with {Non-Line-of-Sight} Perception. In *20th USENIX Symposium on Networked Systems Design and Implementation (NSDI 23)*. 1341–1358.
- [5] Elin Carstensdottir, Nathan Partlan, Steven Sutherland, Tyler Duke, Erika Ferris, Robin M Richter, Maria Valladares, and Magy Seif El-Nasr. 2020. Progression maps: conceptualizing narrative structure for interaction design support. In *Proceedings of the 2020 CHI Conference on Human Factors in Computing Systems*. 1–13.
- [6] Hila Chefer, Yuval Alaluf, Yael Vinker, Lior Wolf, and Daniel Cohen-Or. 2023. Attend-and-Excite: Attention-Based Semantic Guidance for Text-to-Image Diffusion Models. *ACM Trans. Graph.* 42, 4, Article 148 (July 2023), 10 pages. doi:10.1145/3592116
- [7] Minghao Chen, Iro Laina, and Andrea Vedaldi. 2024. Training-free layout control with cross-attention guidance. In *Proceedings of the IEEE/CVF Winter Conference on Applications of Computer Vision*. 5343–5353.
- [8] Oran Gafni, Adam Polyak, Oron Ashual, Shelly Sheynin, Devi Parikh, and Yaniv Taigman. 2022. Make-a-scene: Scene-based text-to-image generation with human priors. In *European Conference on Computer Vision*. Springer, 89–106.
- [9] Martin Heusel, Hubert Ramsauer, Thomas Unterthiner, Bernhard Nessler, and Sepp Hochreiter. 2017. Gans trained by a two time-scale update rule converge to a local nash equilibrium. *Advances in neural information processing systems* 30 (2017).
- [10] Wonjun Kang, Kevin Galim, and Hyung Il Koo. 2023. Counting guidance for high fidelity text-to-image synthesis. *arXiv preprint arXiv:2306.17567* (2023).
- [11] Bowen Li, Xiaojuan Qi, Thomas Lukasiewicz, and Philip Torr. 2019. Controllable text-to-image generation. *Advances in neural information processing systems* 32 (2019).
- [12] Changyang Li, Wanwan Li, Haikun Huang, and Lap-Fai Yu. 2022. Interactive augmented reality storytelling guided by scene semantics. *ACM Transactions on Graphics (TOG)* 41, 4 (2022), 1–15.
- [13] Wanwan Li, Changyang Li, Minyoung Kim, Haikun Huang, and Lap-Fai Yu. 2023. Location-aware adaptation of augmented reality narratives. In *Proceedings of the 2023 CHI conference on human factors in computing systems*. 1–15.
- [14] Yuheng Li, Haotian Liu, Qingyang Wu, Fangzhou Mu, Jianwei Yang, Jianfeng Gao, Chunyuan Li, and Yong Jae Lee. 2023. Gligen: Open-set grounded text-to-image generation. In *Proceedings of the IEEE/CVF Conference on Computer Vision and Pattern Recognition*. 22511–22521.
- [15] Jiayi Liao, Xu Chen, Qiang Fu, Lun Du, Xiangnan He, Xiang Wang, Shi Han, and Dongmei Zhang. 2024. Text-to-image generation for abstract concepts. In *Proceedings of the AAAI Conference on Artificial Intelligence*, Vol. 38. 3360–3368.
- [16] Tsung-Yi Lin, Michael Maire, Serge Belongie, James Hays, Pietro Perona, Deva Ramanan, Piotr Dollár, and C Lawrence Zitnick. 2014. Microsoft coco: Common objects in context. In *Computer vision—ECCV 2014: 13th European conference, Zurich, Switzerland, September 6–12, 2014, proceedings, part v 13*. Springer, 740–755.
- [17] Chang Liu, Haoning Wu, Yujie Zhong, Xiaoyun Zhang, Yanfeng Wang, and Weidi Xie. 2024. Intelligent grimm-open-ended visual storytelling via latent diffusion models. In *Proceedings of the IEEE/CVF Conference on Computer Vision and Pattern Recognition*. 6190–6200.
- [18] Luping Liu, Zijian Zhang, Yi Ren, Rongjie Huang, Xiang Yin, and Zhou Zhao. 2023. Detector guidance for multi-object text-to-image generation. *arXiv preprint arXiv:2306.02236* (2023).
- [19] Ben Mildenhall, Pratul P. Srinivasan, Matthew Tancik, Jonathan T. Barron, Ravi Ramamoorthi, and Ren Ng. 2020. NeRF: Representing Scenes as Neural Radiance Fields for View Synthesis. In *ECCV*.
- [20] OpenAI. 2023. GPT-4 Technical Report. <https://openai.com/research/gpt-4>.
- [21] Quynh Phung, Songwei Ge, and Jia-Bin Huang. 2024. Grounded text-to-image synthesis with attention refocusing. In *Proceedings of the IEEE/CVF Conference on Computer Vision and Pattern Recognition*. 7932–7942.
- [22] Alec Radford, Jong Wook Kim, Chris Hallacy, Aditya Ramesh, Gabriel Goh, Sandhini Agarwal, Girish Sastry, Amanda Askell, Pamela Mishkin, Jack Clark, et al. 2021. Learning transferable visual models from natural language supervision. In *International conference on machine learning*. PMLR, 8748–8763.
- [23] Aditya Ramesh, Prafulla Dhariwal, Alex Nichol, Casey Chu, and Mark Chen. 2022. Hierarchical text-conditional image generation with clip latents. *arXiv preprint arXiv:2204.06125* 1, 2 (2022), 3.
- [24] Robin Rombach, Andreas Blattmann, Dominik Lorenz, Patrick Esser, and Björn Ommer. 2022. High-resolution image synthesis with latent diffusion models. In *Proceedings of the IEEE/CVF conference on computer vision and pattern recognition*. 10684–10695.
- [25] Olaf Ronneberger, Philipp Fischer, and Thomas Brox. 2015. U-net: Convolutional networks for biomedical image segmentation. In *Medical image computing and computer-assisted intervention—MICCAI 2015: 18th international conference, Munich, Germany, October 5–9, 2015, proceedings, part III 18*. Springer, 234–241.
- [26] Chitwan Saharia, William Chan, Saurabh Saxena, Lala Li, Jay Whang, Emily L Denton, Kamyar Ghasemipour, Raphael Gontijo Lopes, Burcu Karagol Ayan, Tim Salimans, et al. 2022. Photorealistic text-to-image diffusion models with deep language understanding. *Advances in neural information processing systems* 35 (2022), 36479–36494.
- [27] Christoph Schuhmann, Romain Beaumont, Richard Vencu, Cade Gordon, Ross Wightman, Mehdi Cherti, Theo Coombes, Aarush Katta, Clayton Mullis, Mitchell Wortsman, et al. 2022. Laion-5b: An open large-scale dataset for training next generation image-text models. *Advances in Neural Information Processing Systems* 35 (2022), 25278–25294.
- [28] Jaskirat Singh, Junshen K Chen, Jonas K Kohler, and Michael F Cohen. 2025. Storybooth: Training-Free Multi-Subject Consistency for Improved Visual Storytelling. In *The Thirteenth International Conference on Learning Representations*. <https://openreview.net/forum?id=JZL0n6cvx8>
- [29] Wenqiang Sun, Teng Li, Zehong Lin, and Jun Zhang. 2024. Spatial-Aware Latent Initialization for Controllable Image Generation. *arXiv preprint arXiv:2401.16157* (2024).
- [30] Zhaorui Tan, Xi Yang, and Kaizhu Huang. 2024. Semantic-aware data augmentation for text-to-image synthesis. In *Proceedings of the AAAI Conference on Artificial Intelligence*, Vol. 38. 5098–5107.
- [31] Xiyu Wang, Yufei Wang, Satoshi Tsutsui, Weisi Lin, Bihan Wen, and Alex Kot. 2024. Evolving storytelling: benchmarks and methods for new character customization with diffusion models. In *Proceedings of the 32nd ACM International Conference on Multimedia*. 3751–3760.
- [32] Jinheng Xie, Yuexiang Li, Yawen Huang, Haozhe Liu, Wentian Zhang, Yefeng Zheng, and Mike Zheng Shou. 2023. Boxdiff: Text-to-image synthesis with training-free box-constrained diffusion. In *Proceedings of the IEEE/CVF International Conference on Computer Vision*. 7452–7461.
- [33] Hui Ye, Xiulong Yang, Martin Takac, Rajshekhar Sunderraman, and Shihao Ji. 2021. Improving Text-to-Image Synthesis Using Contrastive Learning. *The 32nd British Machine Vision Conference (BMVC)* (2021).
- [34] Yu Yuan, Xijun Wang, Yichen Sheng, Prateek Chennuri, Xingguang Zhang, and Stanley Chan. 2024. Generative Photography: Scene-Consistent Camera Control for Realistic Text-to-Image Synthesis. *arXiv preprint arXiv:2412.02168* (2024).

- [35] Jingjie Zeng, Zhihao Yang, Qi Yang, Liang Yang, and Hongfei Lin. 2024. Peeling Back the Layers: Interpreting the Storytelling of ViT. In *Proceedings of the 32nd ACM International Conference on Multimedia*. 7298–7306.
- [36] Cheng Zhang, Xuanbai Chen, Siqi Chai, Chen Henry Wu, Dmitry Lagun, Thabo Beeler, and Fernando De la Torre. 2023. Iti-gen: Inclusive text-to-image generation. In *Proceedings of the IEEE/CVF International Conference on Computer Vision*. 3969–3980.
- [37] Han Zhang, Jing Yu Koh, Jason Baldrige, Honglak Lee, and Yinfei Yang. 2021. Cross-modal contrastive learning for text-to-image generation. In *Proceedings of the IEEE/CVF conference on computer vision and pattern recognition*. 833–842.
- [38] Peiang Zhao, Han Li, Ruiyang Jin, and S Kevin Zhou. 2023. Loco: Locally constrained training-free layout-to-image synthesis. *arXiv preprint arXiv:2311.12342* (2023).
- [39] Yufan Zhou, Bingchen Liu, Yizhe Zhu, Xiao Yang, Changyou Chen, and Jinhui Xu. 2023. Shifted diffusion for text-to-image generation. In *Proceedings of the IEEE/CVF conference on computer vision and pattern recognition*. 10157–10166.
- [40] Yufan Zhou, Ruiyi Zhang, Changyou Chen, Chunyuan Li, Chris Tensmeyer, Tong Yu, Jiuxiang Gu, Jinhui Xu, and Tong Sun. 2022. Towards language-free training for text-to-image generation. In *Proceedings of the IEEE/CVF conference on computer vision and pattern recognition*. 17907–17917.